Original article

Meso–macro-scale computational analysis of boron nitride nanotube-reinforced aluminium and epoxy nanocomposites: A case study on crack propagation

Srikant Padmanabhan[1], Ankit Gupta[1] ⓘ **, Gaurav Arora[2],
Himanshu Pathak[2]** ⓘ **, Ramesh G Burela[1] and
Anant S Bhatnagar[1]**

Abstract

In this paper, an outline of mean-field homogenization and fracture toughness of boron nitride nanotube-reinforced aluminium and epoxy composites have been presented. The meso-scale material modelling has been achieved using Mori-Tanaka and double inclusion homogenization schemes. To examine the effectiveness of Mori-Tanaka and double inclusion schemes, a comparison has been drawn with the rule of mixture. Meso-scale numerical results of boron nitride nanotube-reinforced aluminium and epoxy composites are presented for various design parameters such as aspect ratio and volume fraction of boron nitride nanotubes. The validation studies of the developed transversely isotropic composites model have been documented with the experiments performed and existing literature. Finally, macro-scale fracture toughness simulations incorporating the transversely isotropic properties have been performed using the domain integral method. It is observed that aluminium and epoxy with elastoplastic and viscoelastic nature, respectively, have shown a significant effect on the fracture properties of the composites.

Introduction

Fibre-reinforced composite materials constitute an important class of materials associated with several present industrial applications due to the superior properties over conventional engineering materials. These materials are widely being used to replace conventional materials in areas like aerospace, civil, electronic, and medical engineering. Reinforced composite materials are gaining widespread acceptance due to their high strength to weight ratio with enhanced functionalities.[1] These materials can be put into general use once the effective material properties were obtained and optimize the material according to the desired requirements. Homogenization of heterogeneous materials was one of the first approaches in mechanics to yield effective material response, whereas it was originally developed for elastic problems.[2] Multiscale modelling contributes significantly to

materials design in instances where different levels of a hierarchy of material structure contribute to targeted ranges of material properties and responses.[3,4]

To design these high-performance materials, the first requirement is an appropriate matrix material, and promising results have been effectuated on aluminium alloys and epoxy resins as matrix bases in literature. For instance, Giglio et al.[5] have presented a complete characterization of mechanical properties of Al6061 T6 as far as material hardening and

[1]Mechanical Engineering Department, School of Engineering, Shiv Nadar University, Greater Noida, Uttar Pradesh, India
[2]School of Engineering, Indian Institute of Technology, Mandi, Himachal Pradesh, India

Corresponding author:
Ankit Gupta, Shiv Nadar University SNU, Greater Noida, Uttar Pradesh 201314, India.
Email: Ankit.gupta1@snu.edu.in

fracture locus are concerned. Bastwros et al.[6] studied the effects of graphene dispersion in Al6061 by ball milling technique and observed an enhancement of 47% in flexural strength just by 1.0 wt% graphene reinforcement. Ezatpour et al.[7] investigated the microstructure and mechanical properties of Al6061-nanocomposite, and it was found that for both as-cast and extruded samples, by increasing the amount of nanoparticles, the yield strength and tensile strength increased but elongation decreased. Mercier and Molinari[8] have predicted the macroscopic behaviour of a multiphase elastic–viscoelastic material using the self-consistent and Mori-Tanaka (MT) schemes and demonstrated the efficiency of the different homogenization schemes. White and Kim[9] analysed the development of process-induced residual stresses for graphite/epoxy 3501-6 composite material during the curing process to develop a cure-dependent viscoelastic material model for the composite system. Bai et al.[10] predicted the viscoelastic properties using a three-dimensional unit cell finite element (FE) technique for a composite material with a viscoelastic matrix and transversely isotropic elastic fibres.

After the selection of a suitable matrix for the reinforced composite, the choice of reinforcement is critical for enhancing the inherent mechanical properties. Extraordinary yet distinct features of boron nitride nanotube (BNNT) have triggered great interest in fundamental studies on properties and applications of this exotic material.[11] BNNT was first experimentally found in arc discharge by Chopra et al.[12] in 1995 and have many useful intrinsic properties such as excellent mechanical strength, high thermal conductivity, electrically insulating behaviour, and piezoelectric property.

Homogenization is an efficient technique to predict the macroscopic behaviour of composite materials with reinforcements. In the past, Eshelby's model has been used to examine and calculate the effective material properties of reinforced composites.[13] Mean-field homogenization (MFH) techniques like MT[14] and double inclusion (DI)[15] are widely used at present to evaluate effective material response with multiple phases. A certain amount of uncertainty lies in the range of accuracy of the aforementioned schemes when applied to different sets of material altogether. To measure the effectiveness of MFH schemes applied to reinforced composites, results need to be evaluated over a wide range of parameters like volume fraction index, the aspect ratio (AR) of fibres, orientation of fibres, and initial boundary conditions. Through literature review, it is observed that a good amount of work has been performed on nanocomposites with carbon nanotubes (CNTs) as reinforcement in both polymer and metal matrices with encouraging results, but the analysis of boron nanotubes (BNNTs) as reinforcement in lightweight alloys, and viscoelastic epoxy resins is unexplored in the literature. This provides us a motive to explore the efficacy of BNNTs fibres as a prospective reinforcement by implementing multiscale modelling.

In the light of the above discussion, the present investigation study attempts to compute the effective material response of both epoxy 3501-6 resin and Al6061 T6 reinforced with BNNT fibres through analytical micromechanical field homogenization techniques (MFH) and evaluate the deviation in results over a range of possible combinations. The effect of constituent behaviour that is the non-linear elastoplastic nature of Al6061 T6, non-linear viscoelastic nature of epoxy 3501-6 resin, and the elastic nature of BNNT has been considered for computation purpose. To physically validate the multiscale modelling approach, experimental analysis is performed, and results are presented for comparison. Further, these effective properties are used at the macro-level to analyse fracture behaviour (stress intensity factors (SIF) and J-integral) of the composite with variable fractions of BNNT fibres.

The structure of the paper is as follows. Literature and motivation behind problem selection are presented in Introduction section. Sample preparation and mechanical testing of the samples are presented in Sample preparation and mechanical testing section. The theoretical formulation of the homogenization techniques and the calculation procedure used in the study are presented in The methodology of homogenization schemes and Rule of mixture (ROM) sections. The parametric study is presented in Numerical simulations: Validations, results, and discussion section along with the validations with the literature and experiments performed. Applying the results to a macro-level analysis, a case study on crack propagation is presented in Multiscale crack propagation study section. To interpret the observations, the conclusion for the study is presented in Conclusions section.

Sample preparation and mechanical testing

Sample preparation of epoxy-BNNT and Al-BNNT composites

A commercial resin, i.e. Epoxy 3501-6 (procured from Huntsman, Javanthee Enterprises, Chennai, India) widely used in the aerospace industry and multifunctional amine as a curing agent was used in the experimental analysis. Due to propriety reasons, the manufacturer has not revealed the chemical structure of the resin. It is most commonly known by the organic name as bisphenol A diglycidyl ether.

Ten parts of the curing agent were mixed with 100 parts of resin during preparation as recommended by the manufacturer. Epoxy BNNT composites were prepared by using the centrifugal mixer. For good dispersion of BNNTs, the mixture was stirred for

24 h and bath sonicated afterward for 1 h. The dispersed BNNTs in acetone were vaporized by flowing nitrogen through the mixture at 60 °C. Vacuum oven was used further to dried any remaining portion of acetone at 80 °C for 10 h. The leftover was cooled to room temperature in the presence of nitrogen. The mixture in glass mould was kept at room temperature for 48 h and then cured conventionally at 120 °C for 1 h. Later, it is allowed to cool down to room temperature. The prepared composites were then taken out for post-processing and further for mechanical testing. The preparation steps are presented in Figure 1.

Aluminium pellets of 0.5 mm length and 0.1 mm diameter were crushed into powder of spherical shape with a diameter <10 microns in the mechanical workshop. BNNTs following the same temperature and time parameters as mentioned for epoxy-BNNT samples were dispersed in acetone. Samples with 2% and 3% V_f of BNNTs and aluminium powder were prepared. The composite powder was joined using the cold press at 180 MPa for 15 min and sintered at 580 °C for 1 h. The samples were cooled to room temperature at a constant rate, i.e. 5 °C/min. The preparation details are presented in Figure 2.

Tensile testing of Epoxy-BNNT and Al-BNNT composites

Standard samples of Epoxy BNNT composites were prepared following the ASTM D3039 procedure. Six samples were tested for the reproducibility of results at room temperature. For all samples, the cross-head speed maintained was 1 mm/min. A load cell of 10 kN was used on the universal material testing machine (Instron 5567). As shown in Figure 3(a), the composites have shown linear nature up to 1% strain. ASTM D 3552 was followed to test the prepared Al-BNNT samples. The stress–strain curve for 2% and 3% V_f of BNNT-reinforced aluminium is shown in Figure 3(b). The samples are linear up to 0.05% strain and have shown an increase in ultimate strength with an increase in the volume fraction of BNNTs.

The methodology of homogenization schemes

If the microstructure of reinforced composite consists of two or more phases, then the homogenization of response from each of the phases (matrix and inclusion) to a particular loading is required to get the macro-level response of the resulting new material. Two stages are required to establish the macroscopic response of heterogeneous materials, and the first step being localization problem and consists of solving the problem of an inclusion embedded into an infinite reference homogeneous medium (Eshelby's solution). The second step involves averaging and consists of connecting the local variables to the global ones.[8] The Lielens model (DI), unlike the MT model, is restricted to moderate volume fractions of inclusions (less than 25%), but in practice, it can give good predictions well beyond this range.[16]

This study shall be insightful in determining the range of properties to keep in mind while designing non-conventional materials. It has been observed through experiments as well as through
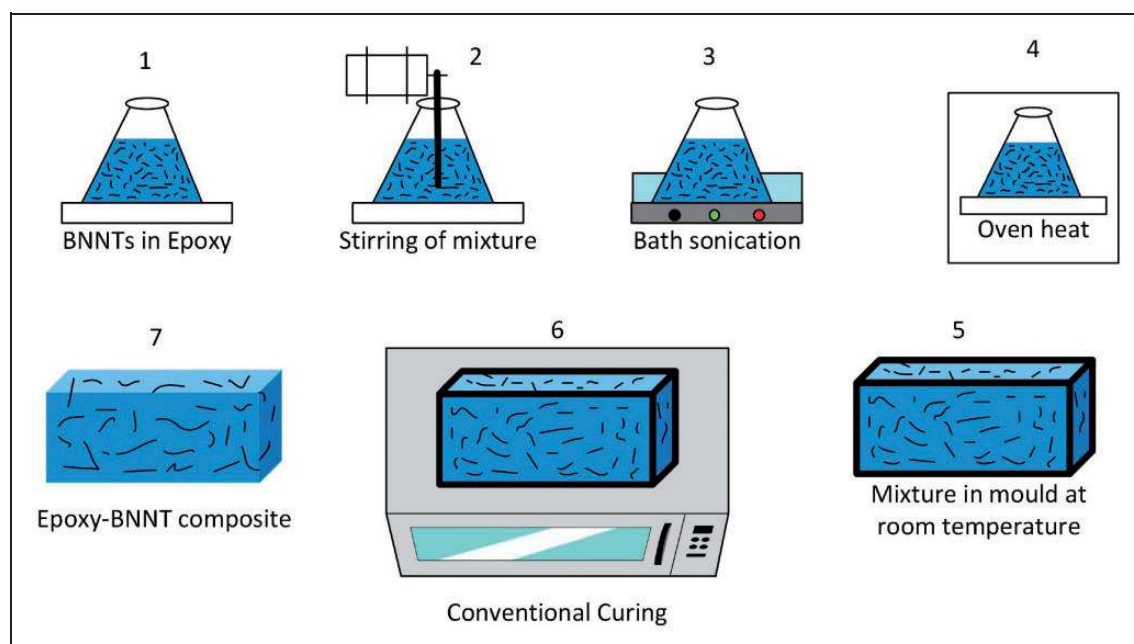

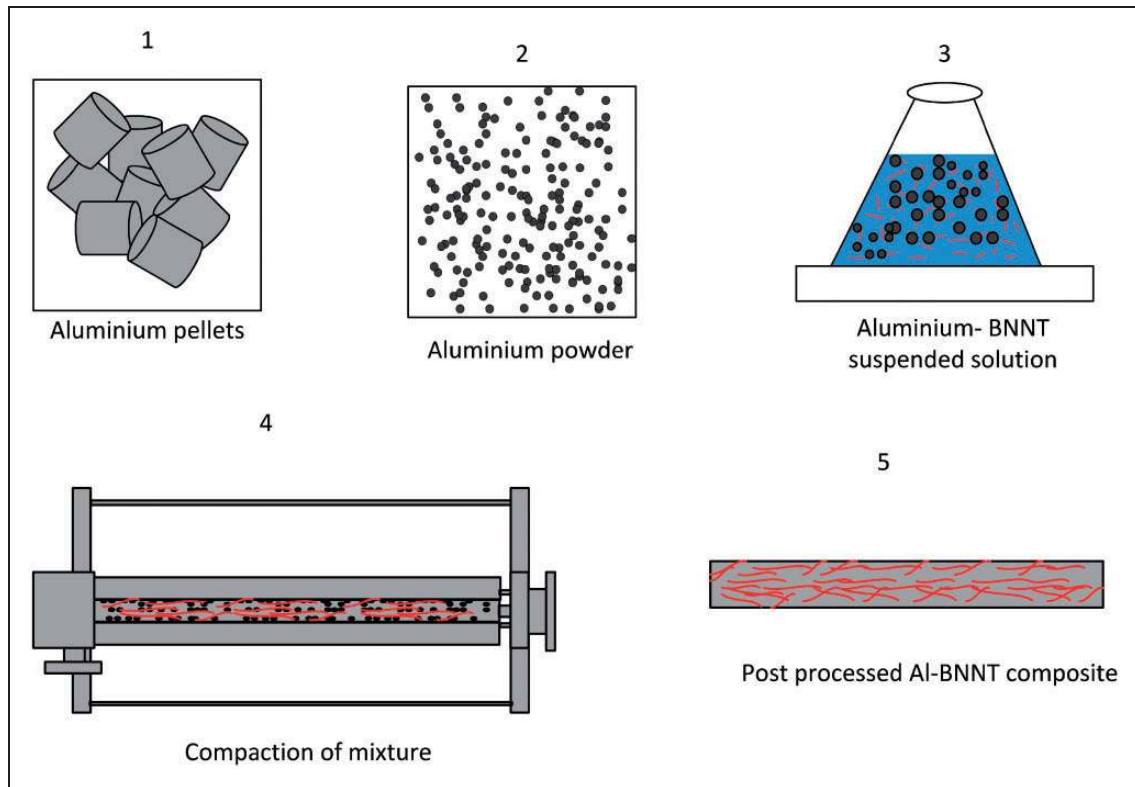**Figure 1.** Preparation of Epoxy-BNNT samples.

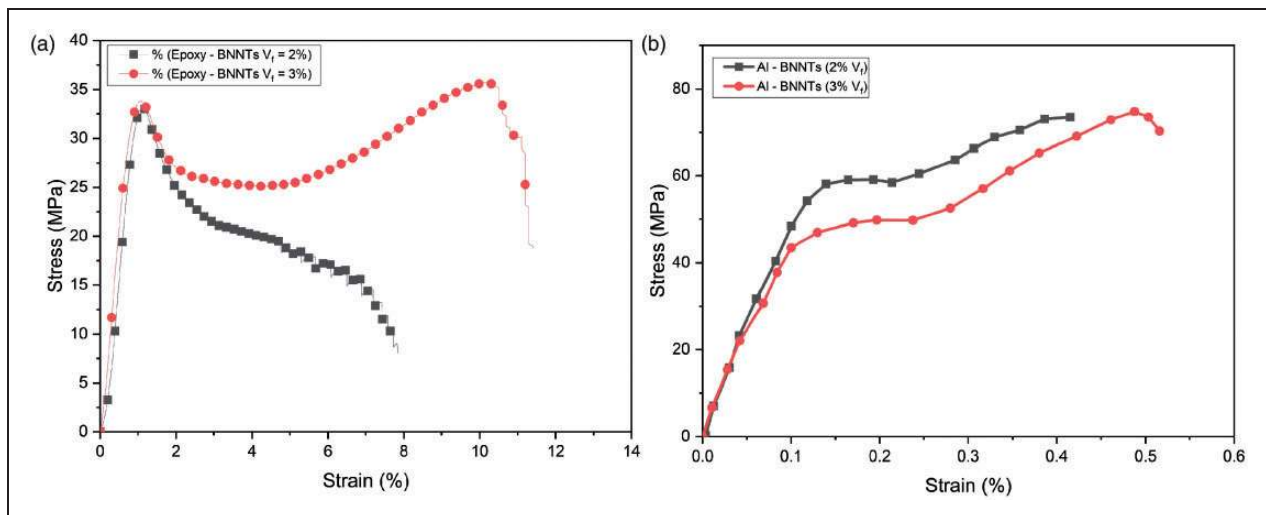**Figure 2.** Preparation of Al-BNNT samples.

Figure 3. Stress–strain curve of (a) Epoxy-BNNTs and (b) Al-BNNTs composites.

computational results that the shape, size, and orientation of the reinforcement play a determining role in deciding the effective material properties of composites. The modelling of reinforced composite material properties for the different cases using the MFH schemes has been achieved with the help of Digimat MF package (version 2018.1), Figure 4[16] illustrates the algorithmic iteration of workflow in Digimat software.

The variation of material properties has been observed by changing certain parameters and subsequent results are presented for reference. In the case of the elastoplastic matrix phase, in all of the considered numerical cases, Poisson's ratio for Al6061 and BNNT has been taken a constant value of 0.33[5] and 0.25,[17] respectively. In the case of the viscoelastic matrix phase, the Prony weights and relaxation times for epoxy resin (3501-6) are considered the
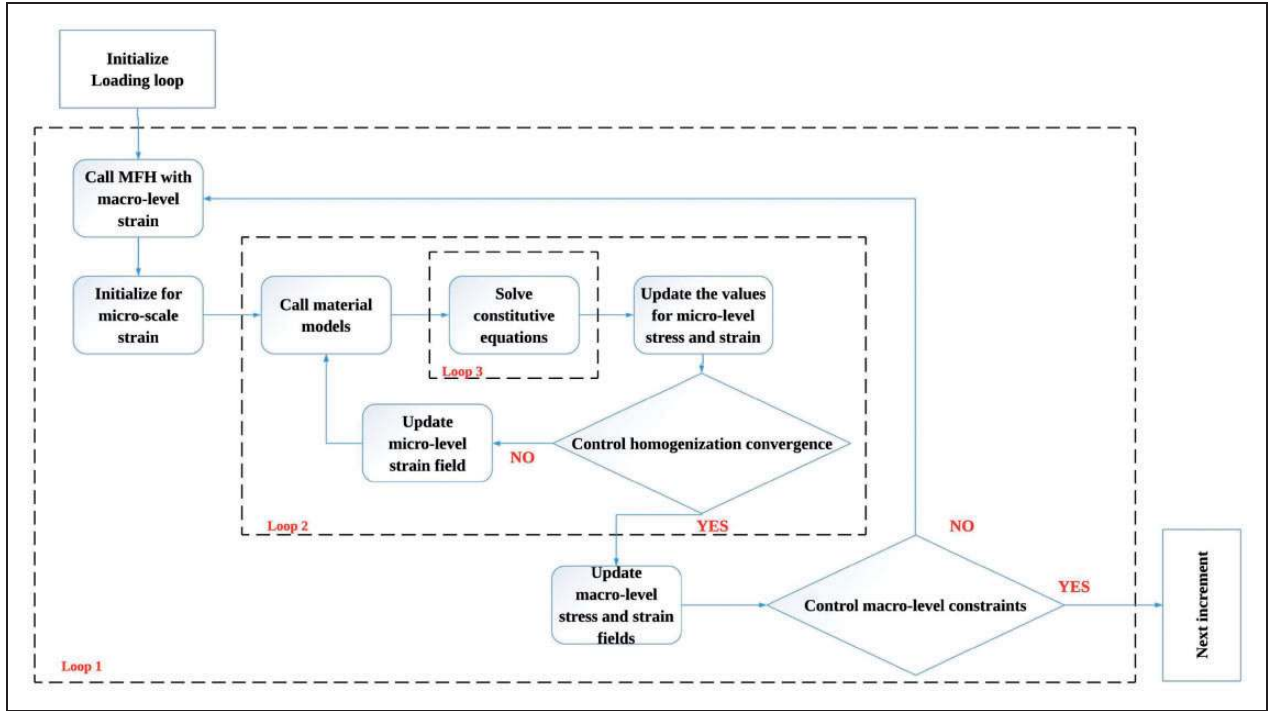
Figure 4. Algorithmic iteration process in Digimat.

same for shear modulus and bulk modulus for all the different considered cases.[10] The representative volume element (RVE) implemented in our problem consists of a two-phase composite, which consists of nano-filler, i.e. BNNT aligned along x-axis embedded in the matrix.

MT model

The MT scheme[14] was originally proposed in 1973, and the modified version was presented by Benveniste[18] for the calculation of effective material properties of multi-phase composites. MT theory is based upon Eshelby's model (1957). The introduction of Eshelby's model was a breakthrough approach in the prediction of effective material properties heterogeneous materials.[19]

The notations for stress and strain concentration tensors being used in the following mathematical formulations are referred from Hill[20] who analysed the case of two isotropic phases firmly bonded together to form a mixture with variable concentration.

The relation between the average composite strain and average inclusion's strain is given by

$$\langle \varepsilon \rangle = \varepsilon^1 \left[I + \xi S^0 (C^1 - C^0) \right] \tag{1}$$

using the relation of strain concentration tensors[20]

$$\langle \varepsilon \rangle^1 = A^{\text{Eshelby}} \langle \varepsilon \rangle \tag{2}$$

$$A^{\text{Eshelby}} = \left[I + \xi S^0 (C^1 - C^0) \right]^{-1} \tag{3}$$

for the case of the MT model, the alternate strain concentration tensor[20] has been applied with the assumption that when there are many inclusion particles in the composite microstructure, the average inclusion strain is given by

$$\langle \varepsilon \rangle^1 = A^{\text{Eshelby}} \langle \varepsilon \rangle^0 \tag{4}$$

$$\hat{A}^{\text{MT}} = A^{\text{Eshelby}} \tag{5}$$

$$A^{\text{MT}} = A^{\text{Eshelby}} \left[(1 - V_i) I + V_i A^{\text{Eshelby}} \right]^{-1} \tag{6}$$

$$C^{\text{eff}} = C^0 + \left[V_i (C^1 - C^0) A^{\text{MT}} \right] \tag{7}$$

after computation of the strain concentration tensor from equation (6), use the equation (7) to get the effective stiffness tensor for the resulting composite.

DI model

The DI model was proposed by Nasser and Hori,[15] and it is based on the following idea. The reinforced composite RVE is replaced with a theoretical model made of a fictitious reference matrix of stiffness C^R in which are embedded inclusions of stiffness C^1 coated with a material of stiffness C^0.[16]

The inclusion (I) and its immediate boundary material have the same AR, symmetry axis, and centre, and their volume ratio equals to that of the inclusion and matrix in the actual reinforced

composite.[21]

$$\left[\hat{A}^{MT}\right]^{-1} = \left[A^{Eshelby}\right]^{-1} = \left[I + \xi^1 S^1 (C^0 - C^1)\right] \quad (8)$$

$$\left[\hat{A}^{Lielens}\right] = \left[(1 - \lambda)\left[\hat{A}^{MT}\right]^{-1} + \lambda\left[\hat{A}^{MT-1}\right]^{-1}\right]^{-1} \quad (9)$$

From equations (6) and (8), substitute the values in equation (9) to get the interpolated value of alternate strain concentration tensor.[19] The alternate strain concentration tensor will be used in equation (7) to get the stiffness matrix, and hence the mechanical properties of the resulting composite. The D-I model usually gives excellent predictions of effective properties over a wide range of inclusion volume fractions, ARs, and stiffness contrasts.

ROM

ROM is an approach for approximate estimation of a composite's material properties based on a volume-weighted average of the properties of different phases (matrix and inclusion phase). The method is cost-effective to find the properties analytically required during a comparative research analysis and provide results within good approximation.

ROM calculates the physical properties without taking into account the AR or orientation of the fibre being reinforced. Applying the mechanics of materials theory, obtain the following expressions for the reinforced composite's properties as[17]

$$E_a = E_i \cdot V_i + E_m \cdot (1 - V_i) \quad (10)$$

$$G_t = \frac{(G_i \cdot G_m)}{(V_i \cdot G_i + V_m \cdot G_m)} \quad (11)$$

$$\nu_t = \nu_i \cdot V_i + \nu_m \cdot (1 - V_i) \quad (12)$$

$$\rho = \rho_i \cdot V_i + \rho \cdot (1 - V_i) \quad (13)$$

Numerical simulations: Validations, results, and discussion

Model validations with the literature

To validate the present formulation, the DI model with first-order homogenization has been implemented to determine the normalized moduli ratio. The ratio of axial young's modulus of reinforced composite with that of the matrix is being computed and compared with the reported results available in the literature as shown in Table 1. In the first case, aluminium has been considered as the base matrix reinforced with BNNT fibres (1.66% V_F). The obtained results are compared with the results based on the molecular dynamics simulation by Cong and Lee[22] to study the mechanical properties of the composites. In the second case, bisphenol-F epoxy resin reinforced with CNT fibres (10% V_F) has been used to compare the results given by Maghsoudlou et al.[23] Maghsoudlou et al.[23] carried-out experimental investigation along with FE-based simulations to yield the results. In the last case, brass reinforced with BNNT fibres (5% V_F) has been taken, and the obtained results are compared with the results obtained by Trivedi et al.[17] Authors employed FE method (FEM) based approach to estimate the effective material properties of reinforced composites.

The results obtained using the present solution methodology are in good agreement with molecular dynamics (MD), FEM, and experimental studies for all the studies considered herewith.

Model validations with the experiments

The tensile strength of the composites has increased with an increase in the volume fraction of BNNTs. Young's modulus found experimentally has been compared with the computational work presented in the study, shown in Figure 5(a). A fair agreement between the experimental and computational work has been found. The computational work does not include the defects produced during the preparation of the samples. Therefore, an average difference of

Table 1. Validation of the current model with existing literature.

	Matrix	Reinforcement	Solution Methodology	Normalized moduli (Ea/Ematrix)
Case 1	Aluminium	BNNT (1.66% V_F)	Molecular dynamics	1.1504[22]
			Present	1.1342
Case 2	Bisphenol-F epoxy resin	CNT (10% V_F)	Experimental	1.1408[23]
			Finite element method	1.2871[23]
			Present	1.2557
Case 3	Brass	BNNT (5% V_F)	Finite element method	1.5240[17]
			Present	1.347

BNNT: boron nitride nanotube; CNT: carbon nanotube.
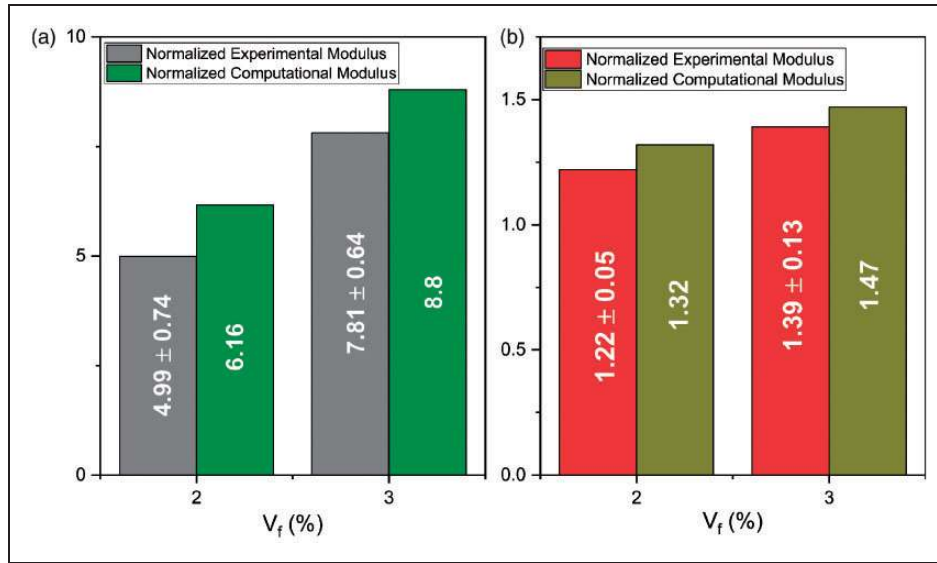
Figure 5. Comparison of experimental and computational longitudinal normalized Young's modulus of (a) Epoxy-BNNT and (b) Aluminium-BNNT composites for AR = 100 of BNNTs.

17.5% can be seen between the two analyses (experimental and computational) for 2% and 3% V_f of BNNTs. The modulus of Al–BNNTs found experimentally has been compared with the computational work presented in Figure 5(b). An average difference of 7% can be seen between the two analysis performed for the samples.

Parametric study

In a reinforced composite, the inclusion's proportion and dimensions of the inclusion play a determining role, and thus the V_F and the AR (length/diameter) of the inclusion phase are varied over a wide range of possible values to investigate the effects of reinforcements on the mechanical properties of the effective composite. The material properties that are being investigated in this study include axial Young's modulus (E_a), transverse Poisson's ratio (ν_t), and transverse shear modulus (G_t).

A summarized comparison between different homogenization schemes applied at different volume fractions (V_F) of inclusion and AR is presented as results. An attempt has been made to establish a comparison between the results for different homogenization techniques and their applicability as well as feasibility under different input parameters. MFH has been employed with two different models namely DI and MT for the determination of effective material properties of reinforced composites in two different matrix environments. The numerical technique of ROM is also implemented in the case of the Al6061 T6 matrix to check its deviation with MFH models. Figure 6[24,25] represents the process flow for the determination of effective material properties and subsequent macro-level modelling employed in ABAQUS/CAE for crack propagation study.

Case 1: Elastic isotropic BNNT is reinforced in the non-linear elastoplastic Al6061 T6 matrix. Continuous elastic fibres of BNNT having an inclusion radius of 1 nm are reinforced in the Al6061 T6 matrix which follows the elastoplastic constitutive laws. J2 plasticity model with linear isotropic hardening (power law) is implemented for the aluminium alloy. First-order DI and MT homogenization schemes with incremental linearization are implemented in Digimat-MF package to obtain the mechanical properties and the stress–strain curve of the reinforced composite. The constituents material proprieties for the reinforcement and the matrix used in the analysis are defined in Tables 2–5. Table 6 shows the computed values at ARs of 100 and corresponding deviations in schemes are also computed for better comprehension. Figure 7 (a) and (b) represents the stress–strain plot for the resulting composite (AR = 100) at different volume fractions, with the fraction of reinforcement increasing and it is seen that the plot tends to be steeper that is the material becomes stiffer and its strength increases. Figures 8 to 10 illustrate the change in properties with a V_F index graphically for AR 350, 550, and 750, respectively, and it is observed that with an increase of volume content of reinforcement there is a linear increase in the value of axial Young's modulus and transverse shear modulus while a linear decrease in the value of transverse Poisson's ratio at all computed ARs of reinforcement.

Implementing ROM as calculated in Table 6 that at an AR of 100 and V_F of 2%, there is a difference of 0.38% in the axial Young's modulus, 1.32% in transverse shear modulus, and 0.13% in transverse Poisson's ratio in comparison to Lielens model. With the same AR of reinforcement and a V_F of 30%, the deviation increases to 0.75% in axial Young's modulus, 24.87% in transverse shear
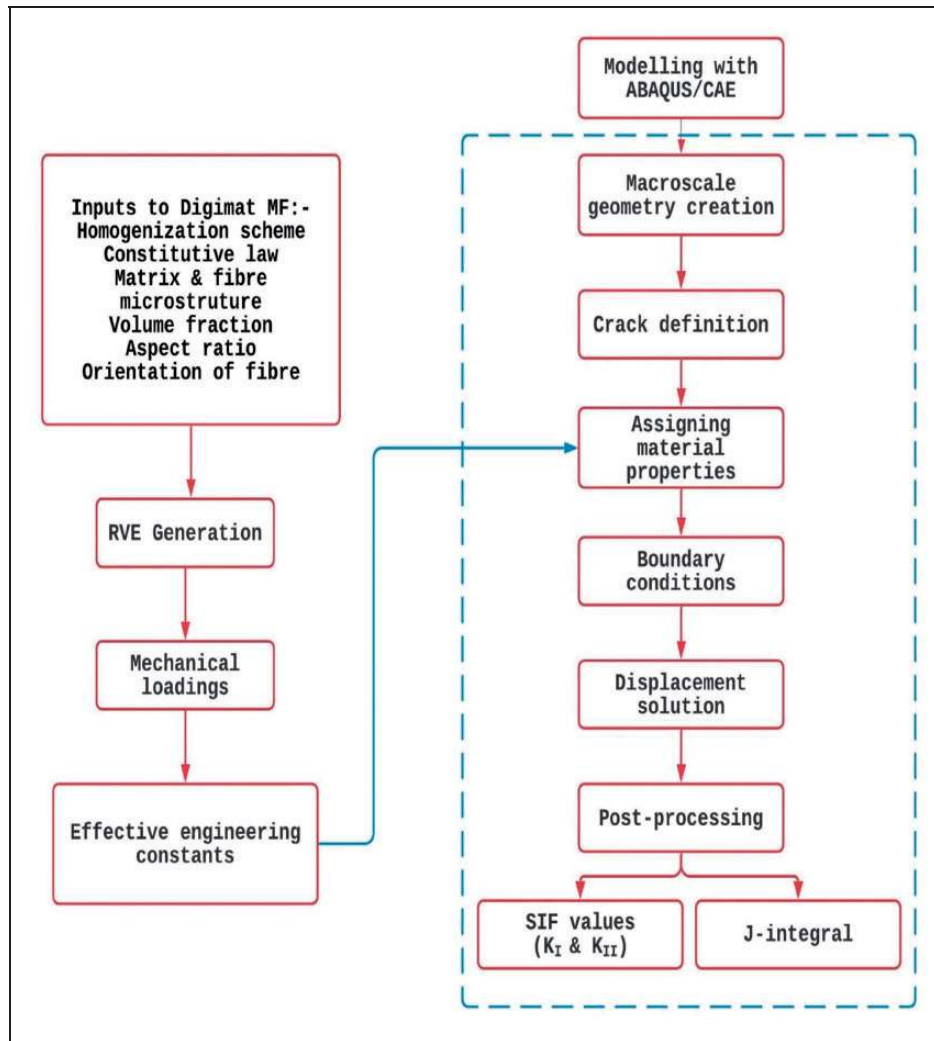
Figure 6. Process flow for computational simulation.

Table 2. Constituent material properties for reinforced composite.

Material	Young's modulus (GPa)	Poisson's ratio	Shear modulus (GPa)	Density (kg/m3)	Constitutive law
BNNT[17]	1180	0.25	500	1400	Elastic
Al6061[26]	68.90	0.33	26.00	2700	Elastoplastic

BNNT: boron nitride nanotube.

Table 3. Elastoplastic properties of Al6061 T6.[23]

|	
Plasticity model	J2
Isotropic hardening model	Power law
Yield stress (MPa)	276
Hardening modulus (MPa)	410
Hardening exponent	0.05

modulus, and 2.39% in transverse Poisson's ratio. This indicates the trend that significant deviation is observed in the results of ROM at higher volume fractions of the reinforcement.

From Table 6, another point to be noted is that different homogenization schemes when applied to transverse direction yield significant differences but when applied to the axial direction result in negligible differences over all the computed volume fractions.

Therefore, it can be estimated for Al6061 T6 reinforced with BNNT, Young's modulus in the axial direction, and transverse Poisson's ratio show little or negligible difference in computed values using different homogenization schemes implemented, but transverse shear modulus shows significant deviation especially at higher V_F of BNNT. It has been found that the numerical model of the ROM is found most inefficient at higher volume fractions of BNNT at all its computed ARs.
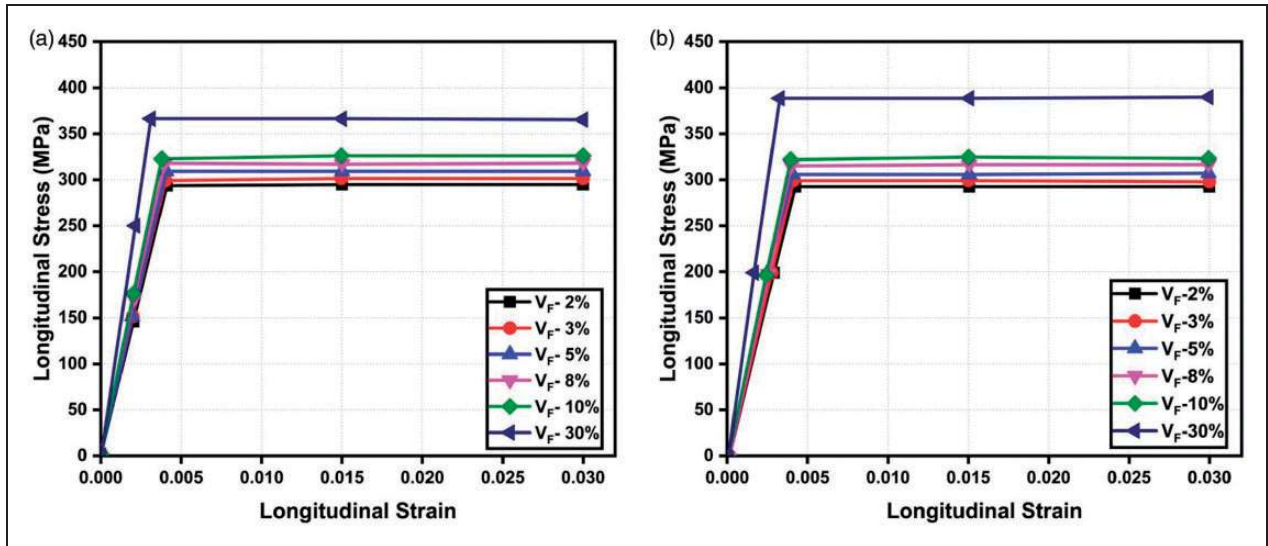
Figure 7. Longitudinal stress–strain plot obtained by (a) Mori-Tanaka and (b) double-inclusion at different volume fractions of BNNT (AR = 100) in the Al6061 T6 matrix.
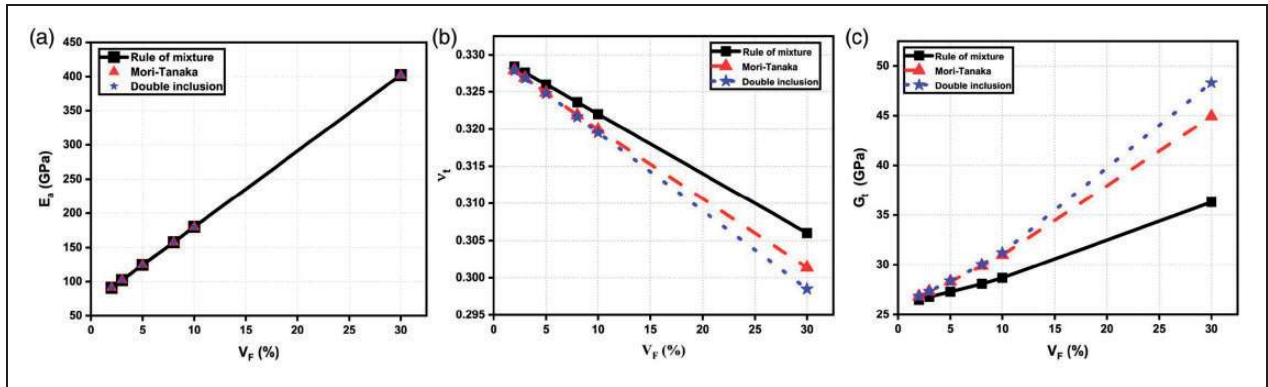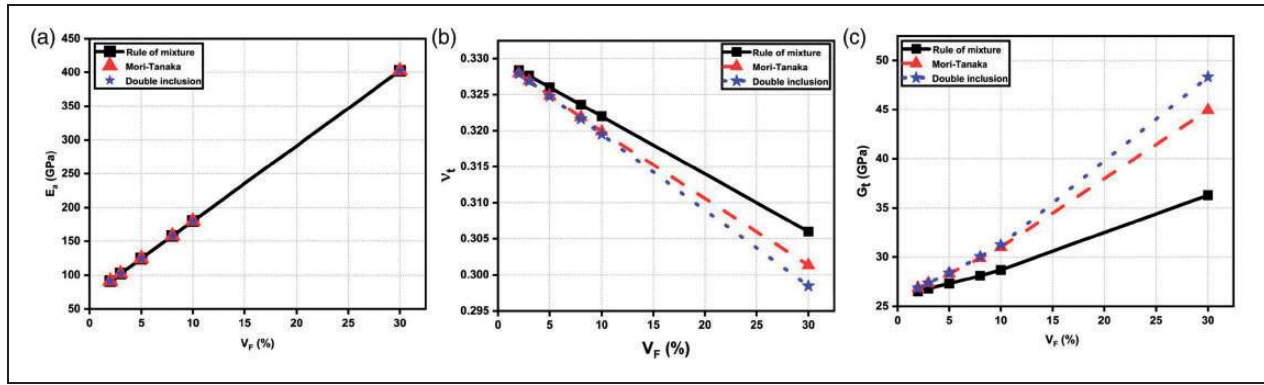

Figure 8. Variation of (a) axial Young's modulus (E_a), (b) transverse Poisson's ratio (ν_t) and (c) transverse shear modulus (G_t) vs volume fraction (V_F) for Al6061 T6 reinforced with BNNT (AR = 350) obtained using different techniques.
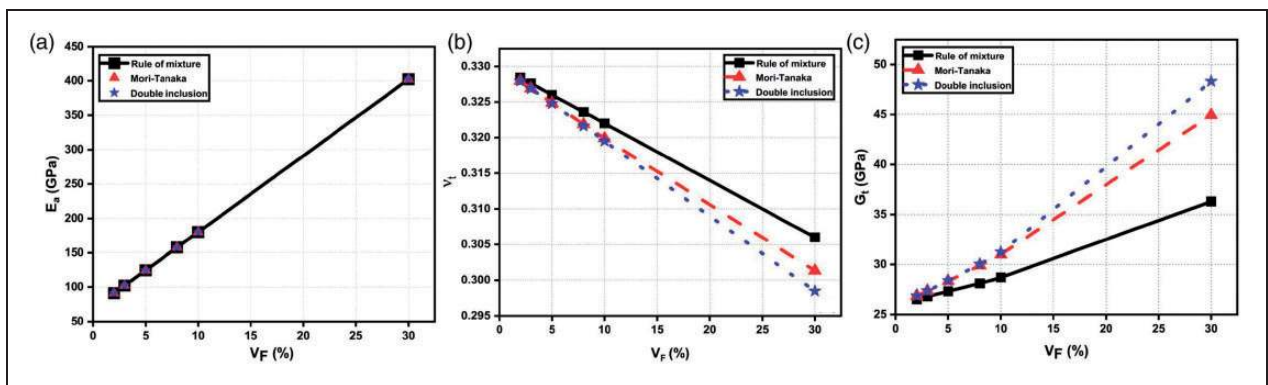
Figure 9. Variation of (a) axial Young's modulus (E_a), (b) transverse Poisson's ratio (ν_t) and (c) transverse shear modulus (G_t) vs volume fraction (V_F) for Al6061 T6 reinforced with BNNT (AR = 550) obtained using different techniques.

Case 2: Elastic isotropic BNNT is reinforced in the viscoelastic 3501-6 epoxy resin matrix. In this case, unidirectional elastic fibres of BNNTs are reinforced within a polymer matrix exhibiting viscoelastic behaviour, i.e. 3501-6 epoxy resin. The input parameters for

accounting viscoelastic nature in the analysis includes a Prony series for shear and bulk modulus.[10] The epoxy 3501-6 resin follows an isotropic viscoelastic behaviour determined by a given set of material properties, and these material constants are assumed to be

Figure 10. Variation of (a) axial Young's modulus (E_a), (b) transverse Poisson's ratio (ν_t) and (c) transverse shear modulus (G_t) vs volume fraction (V_F) for Al6061 T6 reinforced with BNNT (AR = 750) obtained using different techniques.

Table 4. Constituent material properties for epoxy 3501-6 resin and BNNT inclusion.

Material	Young's modulus (GPa)	Poisson's ratio	Shear modulus (GPa)	Density (kg/m3)	Constitutive law
Epoxy resin (3501-6)[10]	3.20	0.35	1.185	1265	Viscoelastic
BNNT[17]	1180	0.25	500	1400	Elastic

BNNT: boron nitride nanotube.

constant with temperature. The input parameters used for this analysis are presented in Tables 4 and 5.

First order DI and MT scheme with incremental linearization is implemented with the help of Digimat MF package, and the properties presented here are for the final state of the matrix after load application. Similar to the case of the Al6061 T6 matrix, there is a linear increase in axial Young's modulus and transverse shear modulus while a decrease in transverse Poisson's ratio. Table 7 represents the mechanical properties at AR of 100 of BNNTs reinforced in aluminium matrix.

The variation in results of the mechanical properties of the MT model in comparison to Lielen's model is calculated to depict the accuracy in the MT model with an increasing V_F index of the inclusion phase. For instance, from Table 7, it has been calculated that for an AR 100 and 2% V_F of inclusion the axial Young's modulus shows a difference of 0.25% and at 30% V_F of inclusion, it is calculated to be 4.53%. The transverse shear modulus shows a difference of only 0.043% at 2% V_F while it increases to 10.98% at 30% V_F. The transverse Poisson's ratio shows a minor increase from 0.0057% at 2% V_F to 1.66% at 30% V_F.

Similarly, at an AR 200 and 2% V_F of inclusion the axial Young's modulus shows a difference of 0.095% and at 30% V_F of inclusion, it is calculated to be 1.54%. The transverse shear modulus shows a difference of only 0.0347% at 2% V_F while it increases to 11% at 30% V_F. The transverse Poisson's ratio shows an increase from 0.0058% at 2% V_F to 1.63% at 30% V_F.

**Table 5.** Prony coefficients for epoxy resin (3501-6).[10]

S. No.	Relaxation time (min)	Prony weights
1	29.20	0.059
2	2.92E+03	0.066
3	1.82E+05	0.083
4	1.10E+07	0.112
5	2.83E+08	0.154
6	7.94E+09	0.262
7	1.95E+011	0.184
8	3.32E+012	0.049
9	4.92E+014	0.025

Figure 11 depicts the stress–strain plot using MT and DI, respectively, for the reinforced composite at different V_F at an AR of 750. In both cases, it is a straight-line plot with an increasing Young's modulus as the V_F of BNNT increases in the matrix phase of epoxy 3501-6 resin. Figures 12(a) to 14(a) depict that the axial Young's modulus results show negligible to no difference, a difference in results of DI and MT for transverse shear modulus, and transverse Poisson's ratio is evident only when V_F of BNNT is above 10% which is depicted in Figures 12(b) to 14(b) and Figures 12(c) to 14(c), respectively.

Thus, it can be predicted for a reinforced–polymer matrix with viscoelastic behaviour, both DI and MT schemes yield excellent results for Young's modulus in the axial direction at all V_F. The Poisson's ratio and shear modulus values in the transverse direction are in good agreeable limits only at lower volume fractions (<10%) of the inclusion in the matrix phase.
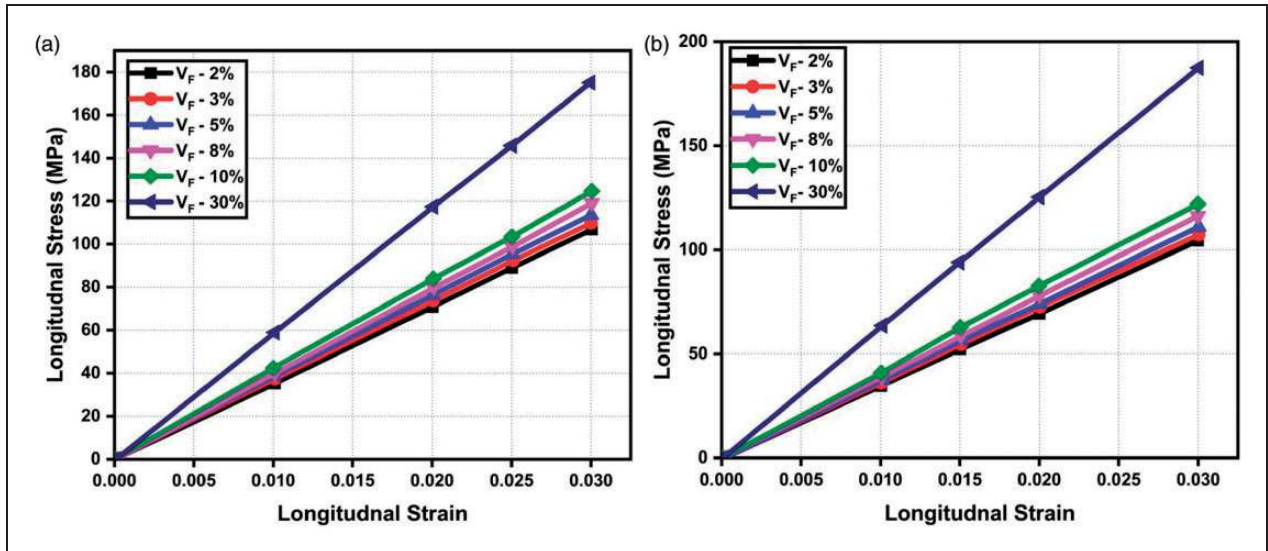
Figure 11. Longitudinal stress–strain plot obtained by (a) Mori-Tanaka and (b) double-inclusion at different volume fractions of BNNT (AR = 750) in 3501-6 Epoxy resin.
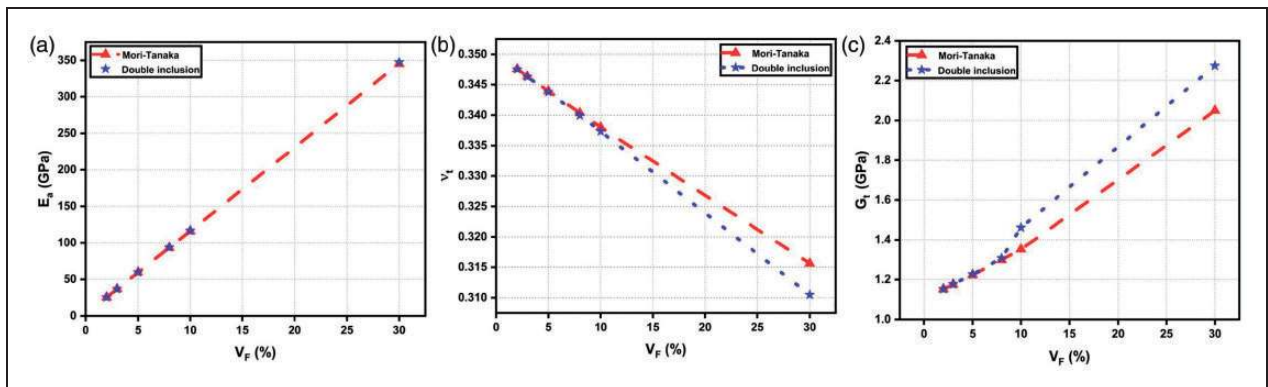
Figure 12. Variation of (a) axial Young's modulus (E_a), (b) transverse Poisson's ratio (ν_t) and (c) transverse shear modulus (G_t) vs volume fraction (V_F) for 3501-6 epoxy resin with BNNT (AR = 350) obtained using different techniques.
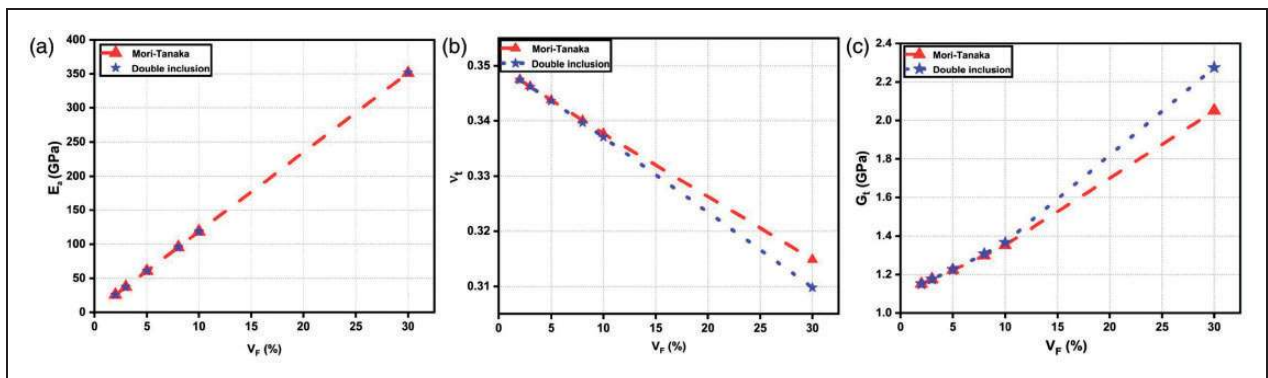
Figure 13. Variation of (a) axial Young's modulus (E_a), (b) transverse Poisson's ratio (ν_t) and (c) transverse shear modulus (G_t) vs volume fraction (V_F) for 3501-6 epoxy resin with BNNT (AR = 550) obtained using different techniques.

Multiscale crack propagation study

A crack propagation analysis is carried out to validate the macro-mechanical response using the domain integral method in the Abaqus CAE package. This would enable us to evaluate the fracture toughness of the material. A rectangular plate having dimensions (100 mm × 50 mm) with an edge crack is

Figure 14. Variation of (a) axial Young's modulus (E_a), (b) transverse Poisson's ratio (ν_t) and (c) transverse shear modulus (G_t) vs volume fraction (V_F) for 3501-6 epoxy resin with BNNT (AR = 750) obtained using different techniques.
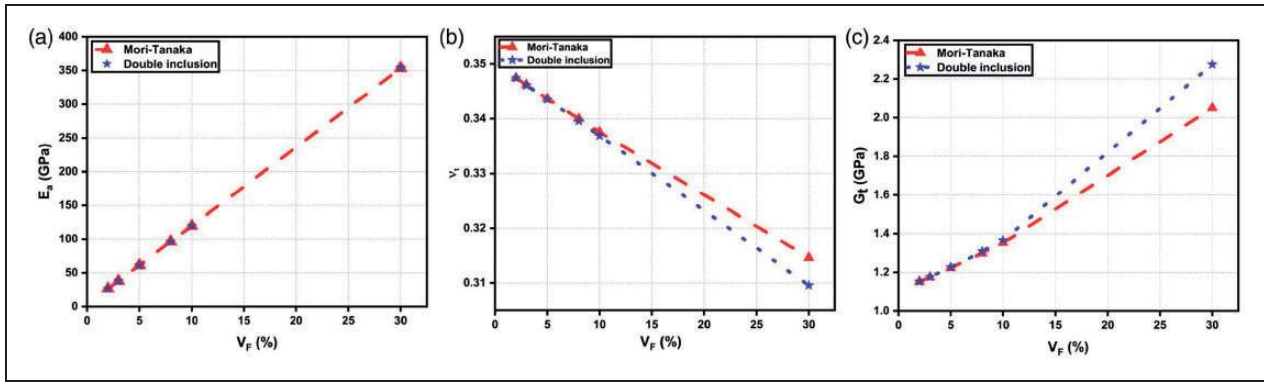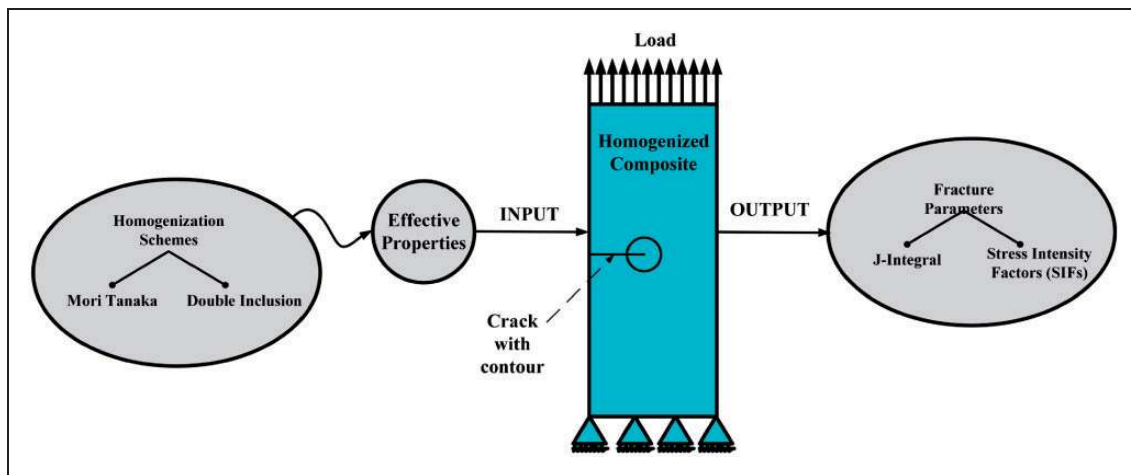

Figure 15. Illustration of multiscale analysis of the composites.

Table 6. Mechanical properties of Al6061 T6 matrix reinforced with BNNT (AR = 100).

AR	V_F (%)	Scheme	E_a (GPa)	ν_t	G_t (GPa)
100	2	ROM	91.1220	0.3284	26.5000
		MT	90.7737	0.3280	26.8480
		DI	90.7770	0.3280	26.8560
		% difference (ROM & MT)	0.3837	0.1311	1.2962
		% difference (MT & DI)	0.0036	0.0030	0.0298
		% difference (ROM & DI)	0.3801	0.1342	1.3256
	3	ROM	102.2330	0.3276	26.8000
		MT	101.7200	0.3270	27.3340
		DI	101.7200	0.3269	27.3520
		% difference (ROM & MT)	0.5043	0.1927	1.9536
		% difference (MT & DI)	0.0000	0.0122	0.0658
		% difference (ROM & DI)	0.5043	0.2049	2.0181
	5	ROM	124.4550	0.3260	27.3000
		MT	123.6100	0.3250	28.3400
		DI	123.6300	0.3249	28.3850
		% difference (ROM & MT)	0.6836	0.3170	3.6697
		% difference (MT & DI)	0.0162	0.0277	0.1585
		% difference (ROM & DI)	0.6673	0.3447	3.8224
	8	ROM	157.7880	0.3236	28.1000
		MT	156.4700	0.3220	29.9050
		DI	156.5400	0.3218	30.0470
		% difference (ROM & MT)	0.8423	0.4907	6.0358

(continued)

Table 6. Continued

AR	V$_F$ (%)	Scheme	E$_a$ (GPa)	ν_t	G$_t$ (GPa)
		% difference (MT & DI)	0.0447	0.0746	0.4726
		% difference (ROM & DI)	0.7972	0.5656	6.4798
	10	ROM	180.0100	0.3220	28.7000
		MT	178.4000	0.3201	31.0040
		DI	178.5000	0.3197	31.2360
		% difference (ROM & MT)	0.9025	0.5999	7.4313
		% difference (MT & DI)	0.0560	0.1157	0.7427
		% difference (ROM & DI)	0.8459	0.7163	8.1188
	30	ROM	402.2300	0.3060	36.3000
		MT	398.4600	0.3018	44.9570
		DI	399.2500	0.2989	48.3150
		% difference (ROM & MT)	0.9461	1.4017	19.2562
		% difference (MT & DI)	0.1979	0.9771	6.9502
		% difference (ROM & DI)	0.7464	2.3925	24.8681

AR: aspect ratio; ROM: rule of mixture; MT: Mori-Tanaka; DI: double inclusion.

Table 7. Mechanical properties of 3501-6 epoxy resin reinforced with BNNT (AR = 100).

AR	V$_F$ (%)	Scheme	E$_a$ (GPa)	ν_t	G$_t$ (GPa)
100	2	MT	19.7160	0.3483	1.1523
		DI	19.7650	0.3483	1.1528
		% difference (MT & DI)	0.2485	0.0057	0.0434
	3	MT	28.1540	0.3475	1.1755
		DI	28.2660	0.3475	1.1766
		% difference (MT & DI)	0.3978	0.0173	0.0936
	5	MT	45.1790	0.3458	1.2234
		DI	45.4950	0.3457	1.2265
		% difference (MT & DI)	0.6994	0.0434	0.2534
	8	MT	71.1102	0.3433	1.2990
		DI	71.9250	0.3429	1.3076
		% difference (MT & DI)	1.1458	0.1107	0.6620
	10	MT	88.6460	0.3416	1.3523
		DI	89.9460	0.3410	1.3664
		% difference (MT & DI)	1.4665	0.1727	1.0427
	30	MT	276.5100	0.3242	2.0508
		DI	289.0600	0.3188	2.2761
		% difference (MT & DI)	4.5387	1.6688	10.9860

AR: aspect ratio; MT: Mori-Tanaka; DI: double inclusion.

simulated both for the pure matrix and with reinforcements, and the AR of BNNT used in the plate is 350. CPS4 4-node bilinear plane stress element has been used to mesh the rectangular laminar plate. Figure 15 shows the integration of two different computational packages to predict the crack propagation in the plate.

The J-integral values and SIFs have been computed for the seventh contour using an edge crack model in Tables 8 and 9. Each contour includes an additional ring of elements surrounding the crack tip. The driving force for a crack to propagate is the decrease in the mechanical energy of the component. The J-integral is a path independent integral useful in non-lin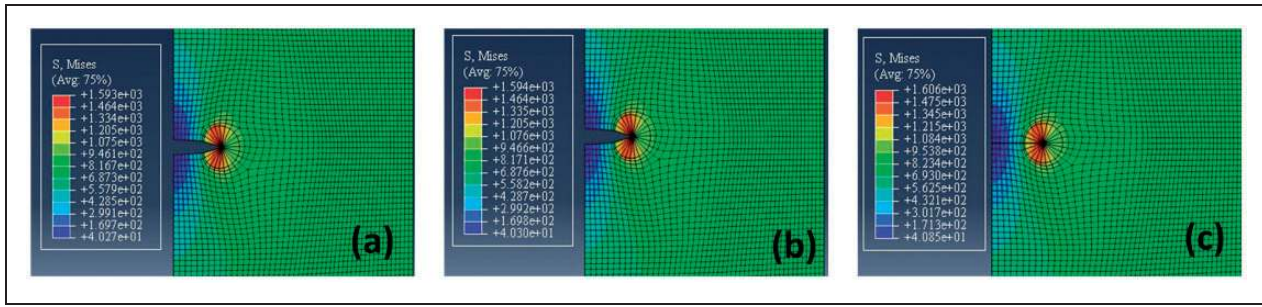ear fracture problems and is used to characterize the energy release rate associated with crack growth. For a virtual crack advance $\lambda(s)$, the energy release rate is given by
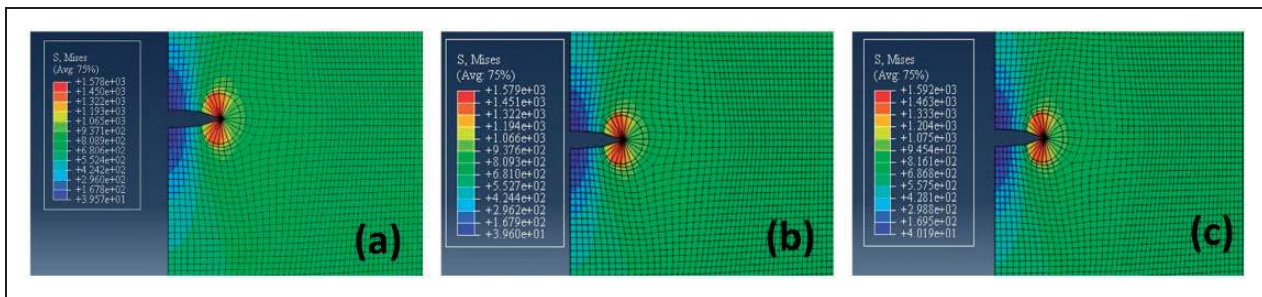
$$J = \int_A \lambda(s)n.H.q\mathrm{d}A \tag{14}$$

where H is given by

$$H = \left(WI - \sigma.\frac{\partial u}{\delta x} \right) \tag{15}$$

The SIFs, K$_I$ and K$_{II}$, are also evaluated to characterize the local crack-tip line stress and displacement fields. It has been seen that the values of SIFs

Figure 16. Contour plots of von Mises stress depicting crack propagation in Al6061 T6 with (a) 0% V_F of BNNT, (b) 2% V_F of BNNT and (c) 30% V_F of BNNT.

Figure 17. Contour plot of von Mises stress depicting crack propagation in epoxy 3501-6 resin with (a) 0% V_F of BNNT, (b) 2% V_F of BNNT and (c) 30% V_F of BNNT.

Table 8. J-integral values for crack propagation using domain integral method.

V_F % (BNNT)	Al/BNNT J-integral (10^{-7} kJ/m^2)	Epoxy/BNNT J-integral (10^{-7} kJ/m^2)
0	2.1605	46.530
2	2.0994	48.231
5	2.0073	45.883
8	1.9164	43.548
10	1.8562	42.003
30	1.2797	27.115

BNNT: boron nitride nanotube.

Table 9. SIFs computed using domain integral method.

V_F % (BNNT)	Al/BNNT		Epoxy/BNNT	
	K_I(Pa$\sqrt{m}$)	$-K_{II}$(Pa$\sqrt{m}$)	K_I(Pa$\sqrt{m}$)	$-K_{II}$(Pa$\sqrt{m}$)
0	136.2	0.3779	135.8	0.3957
2	137.0	0.3753	140.5	0.3723
5	137.8	0.3719	141.4	0.3602
8	138.3	0.3688	141.7	0.3538
10	138.5	0.367	141.8	0.3509
30	139.5	0.3530	142.1	0.3370

BNNT: boron nitride nanotube.

show only a slight increase with the increase of V_F of BNNT fibres in both Al6061 T6 and epoxy 3501-6 resin. They are related to the energy release rate (the J-integral) through

$$J = \frac{1}{8\pi}(K^T.B^{-1}.K) \qquad (16)$$

In the case of Al6061 T6, with the increase of the V_F of BNNT, there is a subsequent decrease in J-integral values for Al6061 T6 for the same load and boundary conditions. The inference that can be drawn from this trend is that the energy release rate at the crack tip in an MMC decreases proportionally with increasing V_F of the reinforcement. Figure 16(a) to (c) illustrates the von-Mises stress plots for different V_F, and it can be seen that the crack propagates both in pure matrix case

as well as with 2% V_F of BNNT reinforcement, but there is no visible crack opening when the V_F of BNNT is increased to 30%. Thus, increasing the inclusion percentage encourages crack resistance in Al6061 T6 reinforced with BNNT fibres.

For the case of epoxy 3501-6, the J-integral value shows an increment at 2% V_F followed by a gradual decrease in values till the V_F of BNNT reaches 30%. The pure epoxy 3501-6 resin with 30% V_F shows the lowest value of energy release rate. With the addition of BNNT inclusions, the strength of the reinforced epoxy 3501-6 resin has increased, but the tendency for crack propagation shows negligible change as shown in Figure 17(a) to (c). Therefore, it can be deduced that despite the fact the strength per unit density for the material has increased with BNNT inclusions, the crack resistance subsequently has increased

slightly in the case of Al6061 T6 while it is negligible in the case of viscoelastic epoxy 3501-6 resin.

Conclusions

In the present work, MFH techniques of MT and DI along with experimental procedure have been implemented for both Al6061 T6 and epoxy 3501-6 matrices with BNNT reinforcements to find the effective material properties. The numerical technique of ROM has also been implemented for the case of Al6061 T6 reinforced with BNNT. This study enables us to find the competence of the homogenization schemes in implementation. It has been validated that the size of the inclusion (AR), its orientation in the matrix, V_F of the inclusion, matrix environment (constitutive law), mechanical properties of the inclusion as well as the matrix play a determining role in the resulting reinforced composite's properties. Fracture toughness parameters are evaluated for a macro-level structure composed of the reinforced composite through a crack propagation study.

The salient outcomes of the study are listed below:

- The BNNT-reinforced composites exhibit transversely isotropic properties.
- With an increasing V_F of the BNNT, there is an increase in the axial Young's modulus, a decrease in transverse Poisson's ratio, and an increase in transverse shear modulus in both Al6061 T6 and epoxy 3501-6 resin matrix composites.
- With an increasing AR of the fibres, there is a corresponding appreciable increase only in the axial Young's modulus in both Al6061 T6 and epoxy 3501-6 resin matrix composites.
- The shape and surrounding medium have a profound effect on the effective material properties of reinforced composites.
- Through the MFH technique, it has been noticed that the results from MT technique are in good agreement with the DI scheme for lower volume fractions of the inclusion, but significant deviations are observed at higher volume fractions. DI scheme has shown fewer errors compared to MT with the existing literature for all volume fractions.
- The numerical technique of ROM provides good approximations in the case of the Al6061 T6 matrix for axial Young's modulus at all volume fractions, but significant differences are encountered in transverse shear modulus and transverse Poisson's ratio.
- Multi-scale modelling has been implemented through the linkage of micromechanical results of Digimat and macro-scale analysis in ABAQUS for crack propagation.
- Crack resistance with BNNT reinforcement increases slightly more in Al6061 T6 in comparison to the epoxy 3501-6 resin matrix.

ORCID iDs

Ankit Gupta https://orcid.org/0000-0002-2961-225X
Himanshu Pathak https://orcid.org/0000-0003-3820-815X

References

1. Rasoolpoor M, Ansari R and Hassanzadeh-aghdam MK. Multiscale analysis of the low-velocity impact behavior of ceramic nanoparticle-reinforced metal matrix nanocomposite beams by micromechanics and finite element approaches. *Proc IMechE, Part L: J Materials: Design and Applications* 2019; 233: 1–14.
2. Geers MGD, Kouznetsova VG, Matouš K, et al. *Homogenization methods and multiscale modeling: non-linear problems*. New York: John Wiley & Sons, 2018.
3. McDowell DL and Olson GB. Concurrent design of hierarchical materials and structures. Sci Model Simulat 2008; 15: 207.
4. Bennoura M and Aboutajeddine A. Predictive capabilities of micromechanical models for composite materials. *J Reinf Plast Compos* 2016; 35: 1115–1125.
5. Giglio M, Gilioli A and Manes A. Mechanical behaviour of Al 6061-T6 aluminium alloy under large strain and failure. In: Bonora N and Brown E (eds) *Numerical Modeling of Materials Under Extreme Conditions. Advanced Structured Materials*, Vol 35, 2014. Berlin, Heidelberg: Springer.
6. Bastwros M, Kim GY, Zhu C, et al. Effect of ball milling on graphene reinforced Al6061 composite fabricated by semi-solid sintering. *Compos Part B Eng* 2014; 60: 111–118.
7. Ezatpour HR, Sajjadi SA, Sabzevar MH, et al. Investigation of microstructure and mechanical properties of Al6061-nanocomposite fabricated by stir casting. *Mater Des* 2014; 55: 921–928.
8. Mercier S and Molinari A. Homogenization of elastic-viscoplastic heterogeneous materials: self-consistent and Mori-Tanaka schemes. *Int J Plast* 2009; 25: 1024–1048.
9. White SR and Kim Y. Process-induced residual stress analysis of AS4/3501-6 composite material. *Mech Compos Mater Struct* 1998; 5: 153–186.
10. Li H, Zhang B and Bai G. Effects of constructing different unit cells on predicting composite viscoelastic properties. *Compos Struct* 2015; 125: 459–466.
11. Kim JH, Pham TV, Hwang JH, et al. Boron nitride nanotubes: synthesis and applications. *Nano Converg* 2018; 5: 17.
12. Chopra NG. Boron nitride nanotubes. *Mater Sci Eng R Report* 2010; 70: 92–111.
13. Withers PJ. The determination of the elastic field of an ellipsoidal inclusion in a transversely isotropic medium,

and its relevance to composite materials. *Philos Mag A Phys Condens Matter Struct Defects Mech Prop* 1989; 59: 759–781.

14. Mori T and Tanaka K. Average stress in matrix and average elastic energy of materials with misfitting inclusions. *Acta Metall* 1973; 21: 571–574.

15. Nasser SN and Hori M. *Micromechanics: overall properties of heterogeneous materials.* Amsterdam, Netherlands: Elsevier, 1969.

16. Digimat. Digimat USER'S MANUAL, www.e-Xstream.com (2017, accessed 12 September 2020).

17. Trivedi S, Sharma SC and Harsha SP. Evaluations of Young's modulus of boron nitride nanotube reinforced nano-composites. *Proc Mater Sci* 2014; 6: 1899–1905.

18. Benveniste Y. A new approach to the application of Mori-Tanaka's theory in composite materials. *Mech Mater* 1987; 6: 147–157.

19. Kassem GA. *Micromechnaicl material models for polymer composites through advanced numerical simulation techniques.* Aachen, Germany: Publikationsserver der RWTH Aachen University.

20. Hill R. Elastic properties of reinforced solids: some theoretical principles. *J Mech Phys Solids* 1963; 11: 357–372.

21. Doghri I and Ouaar A. Homogenization of two-phase elasto-plastic composite materials and structures: study of tangent operators, cyclic plasticity and numerical algorithms. *Int J Solids Struct* 2003; 40: 1681–1712.

22. Cong Z and Lee S. Study of mechanical behavior of BNNT-reinforced aluminum composites using molecular dynamics simulations. *Compos Struct* 2018; 194: 80–86.

23. Maghsoudlou MA, Barbaz Isfahani R, Saber-Samandari S, et al. Effect of interphase, curvature and agglomeration of SWCNTs on mechanical properties of polymer-based nanocomposites: experimental and numerical investigations. *Compos Part B Eng* 2019; 175: 107–119.

24. Arora G and Pathak H. Experimental and numerical approach to study mechanical and fracture properties of high-density polyethylene carbon nanotubes composite. *Mater Today Commun* 2020; 22: 100829.

25. Arora G and Pathak H. Multi-scale fracture analysis of fibre-reinforced composites. *Mater Today Proc* 2019; 18: 687–695.

26. ASM Aerospace Specification Metals Inc. http://asm.matweb.com/search/SpecificMaterial.asp?bassnum = MA6061T6 (accessed 12 September 2020).

Appendix

Notations

$A^{Eshelby}$	strain concentration tensor in Eshelby model
C^0	matrix's stiffness tensor
C^1	inclusion's stiffness tensor
dA	surface element
E_a	axial young's modulus of reinforced composite
G_t	transverse shear modulus of reinforced composite
I	fourth order symmetric identity tensor
J	J-integral
n	outward normal to surface element
q	local direction of virtual crack extension
S^0	matrix's compliance tensor
ν_t	transverse Poisson's ratio of reinforced composite
W	elastic strain energy in an equivalent elastic material
$\langle \varepsilon \rangle$	average composite strain
$\langle \varepsilon \rangle^0$	average matrix strain
$\langle \varepsilon \rangle^1$	average inclusion strain
ξ	fourth rank Eshelby's tensor